Thin Solid Films 706 (2020) 138058

Contents lists available at ScienceDirect

Thin Solid Films

journal homepage: www.elsevier.com/locate/tsf

# Improved film density for coatings at grazing angle of incidence in high power impulse magnetron sputtering with positive pulse

F. Avino*[,a], D. Fonnesu[a], T. Koettig[a], M. Bonura[b], C. Senatore[b], A.T. Perez Fontenla[a], A. Sublet[a], M. Taborelli[a]

[a] CERN, 1211 Geneva 23, Switzerland
[b] University of Geneva, 1211 Geneva 4, Switzerland

ARTICLE INFO

*Keywords:*
Magnetron sputtering
HiPIMS
Positive pulse
Plasma
Superconductivity
Niobium

ABSTRACT

The production of a dense and void-free thin film on large and complex substrates is still a challenge in Physical Vapor Deposition. High Power Impulse Magnetron Sputtering (HiPIMS) with voltage inversion (positive pulse) after the main negative pulse is an attractive alternative to a negatively biased substrate to improve the film properties. In this manuscript, the properties of Nb thin-films deposited on flat Cu samples at different incidence angles with respect to the sputtered Nb target are investigated for various coating techniques. In particular, the results obtained using HiPIMS with the application of a positive voltage are compared with those resulting from negatively biased substrates, using as a reference films coated with the consolidated technique of Direct Current Magnetron Sputtering. Images of the film cross section obtained with a Focused Ion Beam - Scanning Electron Microscope enable to assess film morphology and local thickness, which is compared with the value obtained from X-ray Fluorescence measurements. Differences in the film morphology are highlighted for samples placed perpendicularly to the surface of the sputtered target. A significant densification for HiPIMS in the presence of a positive pulse is observed. The application of this approach to the coatings of superconducting radio-frequency cavities is discussed.

## 1. Introduction

Standard sputtering techniques like Direct Current Magnetron Sputtering [1,2] (DCMS) present limits of application for large and complex substrate geometries. Grounded substrates featuring curved surfaces with alternating concavity are necessarily prone to shadowing and strongly varying incidence angle of the sputtered neutral atoms. Particles impinging at grazing angles lead to self-shadowing with the consequent columnar film growth and presence of voids [3,4]. This has to be avoided in applications such as the Nb coating of Superconducting Radio-Frequency (SRF) cavities [5], where the deposition of a dense, defect and impurity free film is a primary prerequisite to meet the SRF specifications. An improved densification can be obtained by increasing the energy of the atoms impinging the surface and consequently the adatom surface mobility. A sufficiently high amount of ionized sputtered atoms and a mechanism to accelerate them towards the substrate is required. A higher ionization fraction can be achieved with High Power Impulse Magnetron Sputtering (HiPIMS), by delivering a significant transient power during pulses of 10 to 500 μs duration, with a low duty cycle ( < 10%), but keeping the average power equivalent to standard continuous sputtering techniques [6,7]. This approach has been proved to be of interest for many domains, from (CrN)-based hard coatings for the automotive and tooling fields [8,9], to hard wear-resistant coatings for plasma fusion applications [10], high adhesion coatings for steam turbine components [11], antimicrobial nanoparticulate film preparation [12], plasma surface pretreatment [13], solar cell applications [14], temperature sensitive substrates [15], and thin-film coatings of accelerating SRF cavities [16,17]. To efficiently accelerate the metal ions, a negative bias can be applied to the substrate [18–21]. However, the application of a negative voltage needs an additional power supply and presents practical limitations in the case of large objects, in particular when the vacuum chamber is itself the substrate to be coated. This is the case for SRF applications and it requires magnetrons with a dedicated design to allow the flow of electrons out of the system. The inversion of the voltage after the negative pulse (positive pulse - PP) [22,23] is an alternative approach under investigation that would allow much simpler designs of the sputtering sources and of the coating setups, finding also application for the coating of non-conducting substrates [24–26]. Several studies on the physics of HiPIMS discharges have been performed [27–31], with

* Corresponding author.
*E-mail address:* fabio.avino@cern.ch (F. Avino).

https://doi.org/10.1016/j.tsf.2020.138058
Received 30 September 2019; Received in revised form 15 April 2020; Accepted 17 April 2020
Available online 26 April 2020

recent results showing the ion energy distribution shift in HiPIMS plasmas with a PP [32,33]. First investigations on the effect of the PP on coated films have been conducted [23,34], but the effective densification of the films in the presence of a PP at grazing incidence angles of the sputtered atoms onto the substrate surface has not been shown yet.

In this manuscript, we analyze Nb thin-films on Cu, coated in Ar with different techniques. Coatings in DCMS with and without a biased substrate, HiPIMS with and without a biased substrate, as well as with a PP are investigated. Samples at 0° and 90° angles of incidence are analyzed. In Section 2, we detail the experimental setup. In Section 3, Ion-Energy Distribution Functions (IEDFs) at the position of the substrate are presented. Film properties are discussed in Section 4, mainly focusing on film morphology by cross section profiles with Focused Ion Beam - Scanning Electron Microscope (FIB - SEM). In Section 5, the specific application of the herein results for SRF cavities is discussed, including the measurements of the superconducting critical temperature of the thin films. Conclusions are summarized in Section 6.

## 2. Experimental setup

The experimental setup for the ion mass and energy measurements is similar to that presented in Avino et al. [32], where more details are available. A magnetron with a medium-balanced magnetic configuration, without magnetic field lines connecting directly the target surface and the substrate, is installed at 15° with respect to the horizontal plane, inside a 43 cm high vacuum chamber. The magnetic null-point is located ~ 3.5 cm from the Nb target, which has a diameter of 50 mm and a thickness of 2 or 3 mm. Above the target at a distance of 1 mm, a grounded guarding ring acts as an anode and covers the outer 2 mm of the target surface. The sputtering process is run in Ar at 0.8 Pa. An ion mass and energy analyzer (MEA) is vertically installed to measure the species and the energy of the collected ions, as depicted in Fig. 1(a). The MEA is mainly composed of a cylindrical energy analyzer and a quadrupole mass analyzer through which ions are selected after the 100 µm wide entrance orifice of the extraction hood (EH). The EH is located along the normal to the target surface at 145 mm from it, as indicated in Fig. 1(b), within 5 mm accuracy and with a 15 ° incidence angle. With the implemented ion optics parameters, the acceptance angle resulting from SIMION 8.1 simulations [32] varies between 15 ° for 10 eV, to less than 3 ° for energies above 20 eV. However, energies higher than 10 eV can be measured because of the acceleration mechanism discussed more in detail in Section 3. A support for Cu samples is installed on the top of the EH through which it can be externally biased with respect to the common ground potential. Cu samples of 10 × 30 mm or 10 × 20 mm, 1 mm thickness are used as substrates and installed at 0° and 90° with respect to the surface normal of the target, as depicted in Fig. 1(b). DCMS plasmas are obtained with a standard DC power supply that can be also connected in series with a 2 kW HiPIMS module. This device allows to generate pulses from the input DC power, and it also provides the flexibility to introduce a PP at the cathode with respect to the common ground potential. with adjustable duration, amplitude, and delay after the main pulse (MP). Voltage and current measurements are directly available on the HiPIMS module. In addition, a high-voltage probe (4 kV) with 400 MHz bandwidth, and a current probe limited to 30 A and 100 MHz bandwidth are implemented to monitor specific features of the HiPIMS discharges requiring a higher time-response, such as the current inversion in the presence of the PP. The parameters kept constant for the explored configurations are the repetition rate of 1 kHz in HiPIMS and the DC power of 250 W, which is reduced between 20 to 30% by the HiPIMS module. The voltage amplitude used for the continuous substrate biasing is −50 V, while that for the PP is +50 V and +100 V. The MP duration of the HiPIMS discharges without PP is 30 µs (3% duty cycle), as shown in Fig. 2. With the inclusion of the PP, coatings with a MP duration of 38 µs are also performed to compensate for the delay in the ramp-up current of ~ 8 µs, as discussed in Avino et al. [32]. This approach was chosen with the aim of keeping a

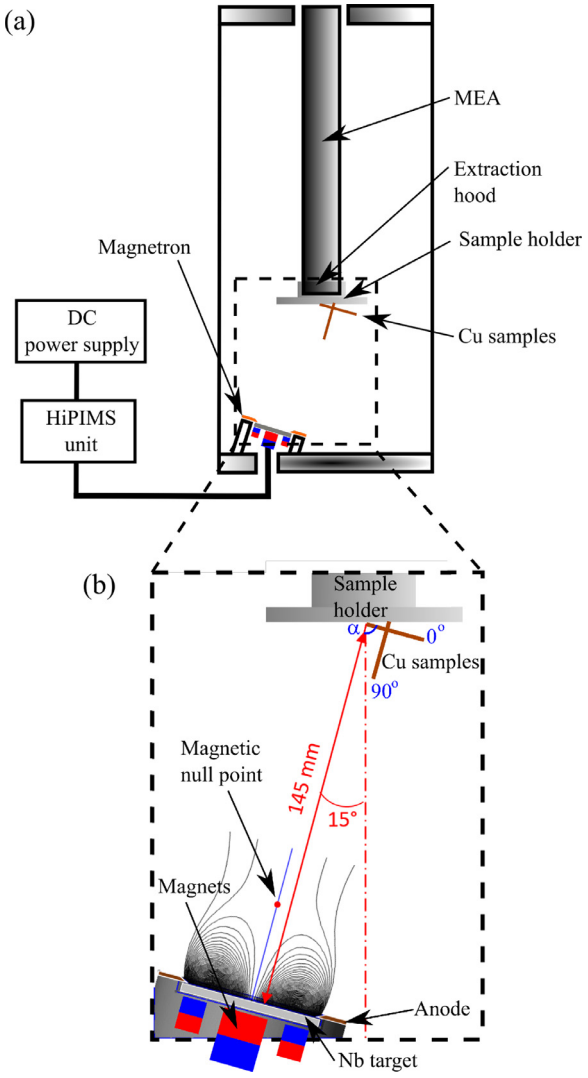


**Fig. 1.** (a) Schematic of the experimental setup. (b) Detail of the setup including the sputtering source and the sample holder. The magnetic configuration is indicated with black-curved lines, while the red dot refers to the magnetic null-point.

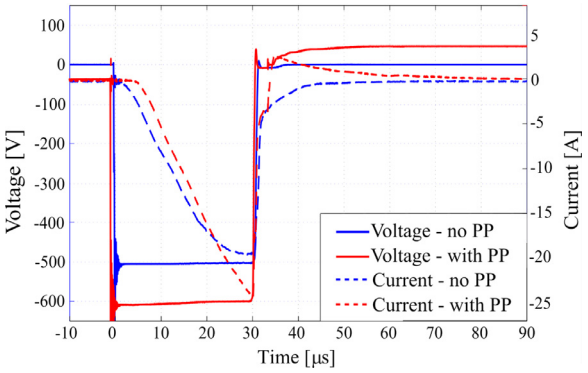


**Fig. 2.** In continuous and dashed lines, respectively, the applied voltage pulse of 30 µs and the corresponding discharge current for different configurations: without PP (blue), and with PP of +50 V and 200 µs (red). The signals are measured with external probes and averaged over 50 pulses to improve the signal-to-noise ratio.

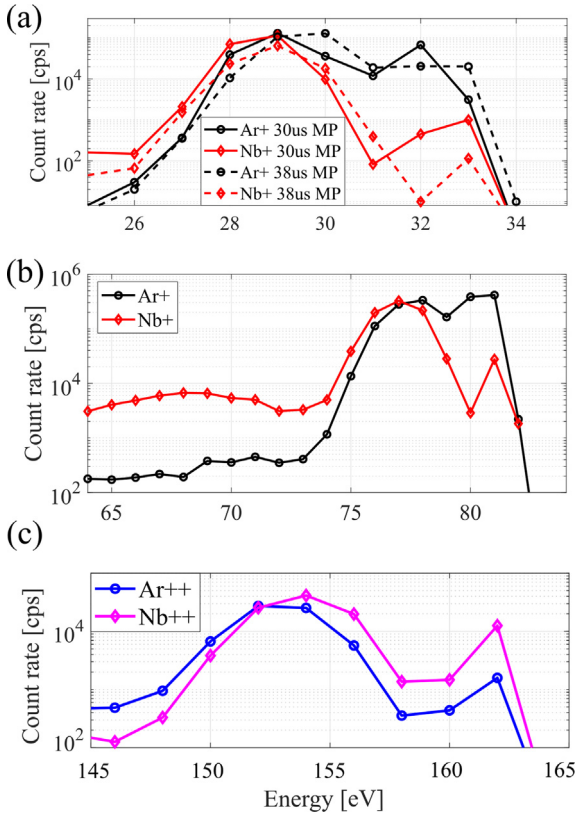


**Fig. 3.** IEDFs of single and double-ionized Ar and Nb atoms with the application of a +50 V PP (a), and +100 V PP (b). In (c), the double-ionized Ar and Nb atoms for the +100 V PP case.

consistent current profile, but no significant differences could be underlined in the results between the coatings with 30 μs and those with 38 μs MP, as well as for the IEDFs, as evident in Fig. 3. A delay of 4 μs and a duration of 200 μs were set for the PP.

## 3. Ion energy distribution functions

The application of a PP after the MP aims at accelerating towards the substrate the metallic and gaseous ions produced in the HiPIMS discharge. The associated ion energy was investigated in previous works for a fixed PP voltage amplitude and variable duration [32] as well as for a variable PP voltage amplitude and fixed duration [33]. In Fig. 3(a) and (b) we report the IEDFs of the single-ionized atoms for the two values of investigated PP amplitudes of +50 V, and +100 V with 4 μs delay and 200 μs duration. For +50 V PP the IEDFs of $Ar^+$ and $Nb^+$ for both the 30 μs and the 38 μs MP are presented, indicating only minor differences. We can observe that the maximum for all the investigated species is close to 29 eV for the +50 V PP and close to 77 eV for the +100 V PP. As discussed in Avino et al. [32], the application of the PP is expected to shift the plasma potential with respect to the reference ground to values close to the PP amplitude, leading to an acceleration of the ions in the plasma sheath. This has a major role in allowing the measurements of ions with energies above 10 eV, given the geometry of the setup, according to the acceptance angle discussed in Section 2. The measured values of ion energies lower than the PP amplitude could be related to the geometry of the system and to the spatial distribution and temporal evolution of the plasma potential during the afterglow. In Fig. 3(c) the IEDFs of the double-ionized species $Ar^{++}$ and $Nb^{++}$ for the +100 V PP are shown, exhibiting as expected a peak kinetic energy at the substrate twice as high as that of the single-ionized atoms ($Ar^+$ and $Nb^+$), but a maximum count rate that is on average one order of magnitude lower. It was verified that a negligible count rate was measured in the energy range lower than that shown in Fig. 3, confirming the complete shift of ion energies as a consequence of the implementation of the PP as discussed in Avino et al. [32].

**Table 1**
Nb/Cu coated films thicknesses at 0° and 90° degrees incidence angles.

| | | | 0° | | 90° | |
|---|---|---|---|---|---|---|
| | | | XRF | FIB-SEM | XRF | FIB-SEM |
| Process | Sub. Bias [V] | PP [V] | Thickness [μm] | | | |
| DCMS | 0 | – | 1.5 | 1.6 | 0.6 | 1.3 |
| DCMS | −50 | – | 1.9 | 1.9 | 0.6 | 1.3 |
| HiPIMS | 0 | 0 | 2.1 | 2.1 | 0.7 | 1.3 |
| HiPIMS | −50 | 0 | 2.0 | 2.0 | 0.7 | 0.8 |
| HiPIMS | 0 | +50 | 2.0 | 2.2 | 0.7 | 0.8 |
| HiPIMS | 0 | +100 | 1.9 | 1.9 | 0.7 | 0.9 |

## 4. Thin-film morphology

In this section, morphological properties of the Nb thin films deposited onto Cu samples are presented. We compare standard DCMS coatings, with the substrate negatively biased or grounded, to HiPIMS coatings with a negatively biased substrate or grounded with a PP of + 50 V and + 100 V. In particular, differences between films coated with the substrates at 0° and 90° with respect to the sputtering target are highlighted. Since grazing angles of incidence are prone to the formation of voids during the film growth [3,4], substrates at 0° and 90° enable to explore the two extreme configurations for the growth of a dense film. The coating times of 1.5 h for the DCMS, and 4 h for the HiPIMS, are chosen to obtain comparable film thickness. In Table 1, the main coating parameters and resulting film thicknesses are summarized.

Films thickness is first obtained with XRF analysis by using a XDAL Fischerscope X-ray system. To guarantee measurements at the same location with respect to the target for all the samples, the analysis is performed at the center of the 10 × 30 mm samples, and at 15 mm from the short edge closer to the sample holder for those 10 × 20 mm, within 1 mm uncertainty. Samples at 0° feature a thickness in the range 1.5–2 μm. For samples at 90° the thickness is reduced by a factor of ~ 3 to 0.6–0.7 μm. FIB-SEM cross sections are performed with a Zeiss XB540 (FIB-SEM cross beam system) to investigate the microstructures of the coated films. The setup is equipped with a gas injection system for FIB-induced Chemical Vapor Deposition, and the InLens detector is used for the conventional SEM imaging. A platinum polishing barrier is first deposited onto the sample surface at a current of 300 pA to facilitate effective polishing. A milling current of 7 nA and accelerating voltage of 30 keV is then used to mill out a 25 × 8 × 8 $\mu m^3$ trench along the long side of the samples, at 15 mm from the short side. Final polishing is performed at a milling current of 700 pA and accelerating voltage of 30 keV to leave a smooth surface that could be effectively imaged. The imaging parameters resulting from an optimization process are 150 pA and 1.5 kV, with nominal magnifications of 25.000 × and 40.000 × .

Fig. 4 shows the cross sections of the films obtained with an incident angle of 0°. Independently of the process (DCMS or HiPIMS), a dense microstructure is observed, with nanometric equiaxial grains out of which V-shape columns have grown up perpendicular to the substrate plane. The columns are composed of various elongated grains. Thickness values confirm within 10% those provided by XRF. In films coated with 90° of incident angle, the above-mentioned columns are oblique as observable in Fig. 5, because of the shadowing that takes place during the film growth [3]. The structural angles are estimated between 60° and 85°. However, depending on the implemented process, significant differences in the porosity of the films can be observed. Specimens produced by DCMS in Fig. 5(a) and (b) show a dominant intergranular

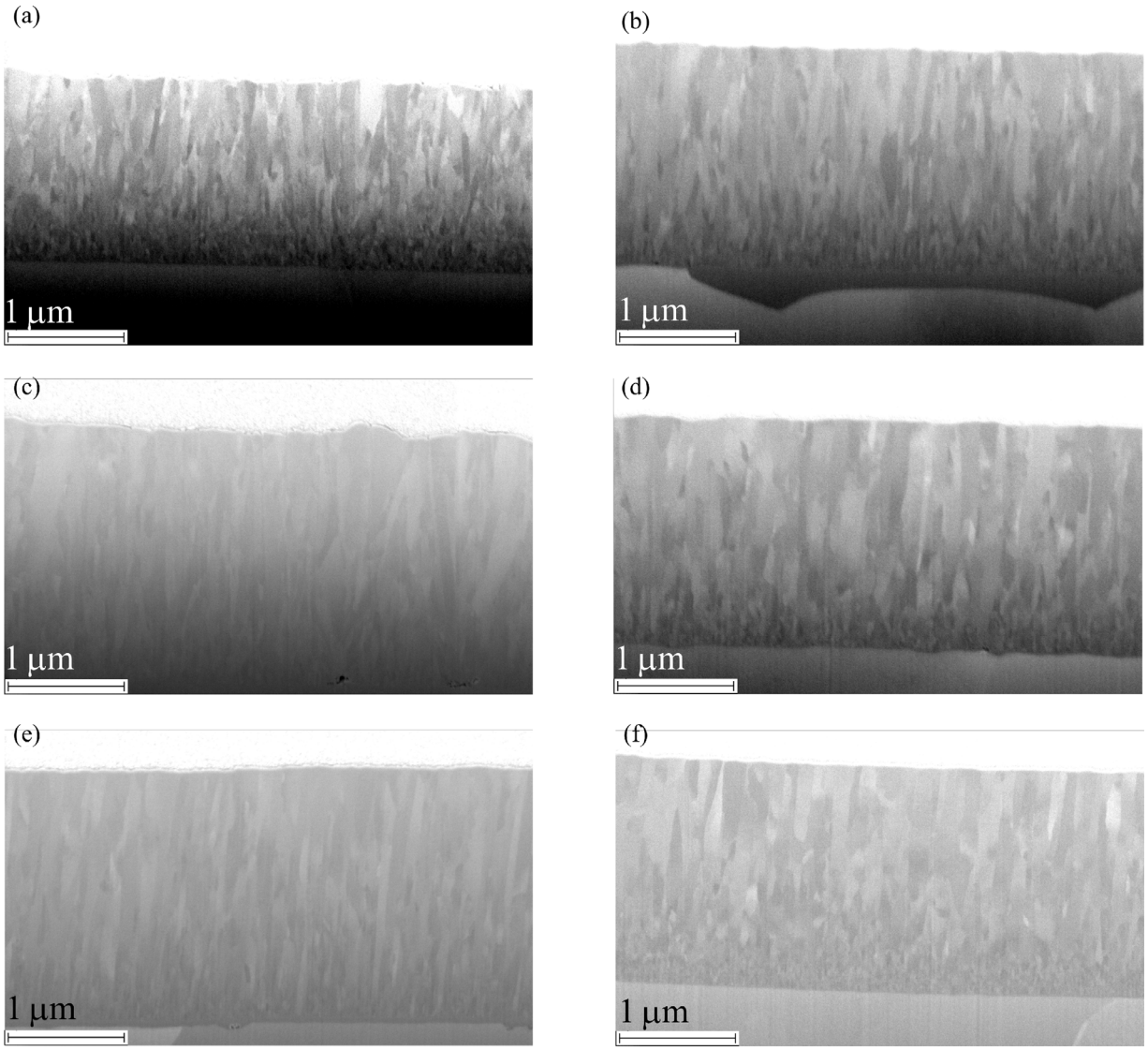


**Fig. 4.** Nb films FIB cross sections of samples at 0° coated in: (a) DCMS with grounded substrate, (b) DCMS with −50 V biased substrate, (c) HiPIMS with grounded substrate, (d) HiPIMS with −50 V biased substrate, (e) HiPIMS with grounded substrate and +50 V PP, (f) HiPIMS with grounded substrate and +100 V PP.

porosity where the columns are completely separated at the grain boundaries. We note in Fig. 5(b) that the film densification is not improved by applying a bias to the substrate in DCMS, since the fraction of metal ions accelerated towards the substrate is very limited. In HiPIMS, the metallic ion flux fraction is larger than in DCMS. However, a film characterized by a columnar growth is still obtained in HiPIMS if the substrate is kept grounded, as shown in Fig. 5(c). This is due to the low energy of the metallic ions impinging the substrate that does not improve the adatom surface mobility to densify the film during the growth. Film thicknesses measured with XRF are strongly underestimated (down to 50%) for these configurations of DCMS with and without biased substrate, and HiPIMS with grounded substrate. This is inherent to the XRF measurement technique in which the model is based on bulk density, therefore explaining the large deviation for porous films.

If a bias of −50 V is applied to the substrate in HiPIMS, $Nb^+$ ions are expected to be accelerated through the plasma sheath before reaching the substrate. This results in a denser film, as can be observed in Fig. 5(d). Finally, in Fig. 5(e) and (f) we present the FIB-SEM results for films produced by HiPIMS with a grounded substrate, but with the addition of a PP of, respectively, +50 V and +100 V PP. The film obtained with a PP of +50 V shows a micro-structure qualitatively comparable to the one obtained with a biased substrate of −50 V. This confirms that the application of the PP and the biased substrate lead to similar effects in terms of a dense film growth for substrates at grazing angles of incidence. We note that the effective 29 eV energy of ions reaching the substrate with the +50 V PP is very likely lower than that with the −50 V substrate bias, for which the ions should get through the substrate sheath an energy close to 50 eV. The lower film surface roughness that can be observed in Fig. 5(e) with respect to Fig. 5(d) could be explained by the different local substrate surface roughness. By increasing the PP voltage to +100 V, the film densification is further increased and the surface roughness is reduced, as visible in Fig. 5(f). These effects can be ascribed to the energetic Nb ions bombarding the surface at 77 eV. The dominant role of high-energy metal ions with respect high energy gas ions in the densification of the films can be ascribed to the more efficient momentum transfer by maximizing the ion energy deposited into the film, therefore providing the energy necessary to eliminate film porosity at low deposition temperatures [21,35].

## 5. SRF application

The film morphology with respect to the incidence angle of the

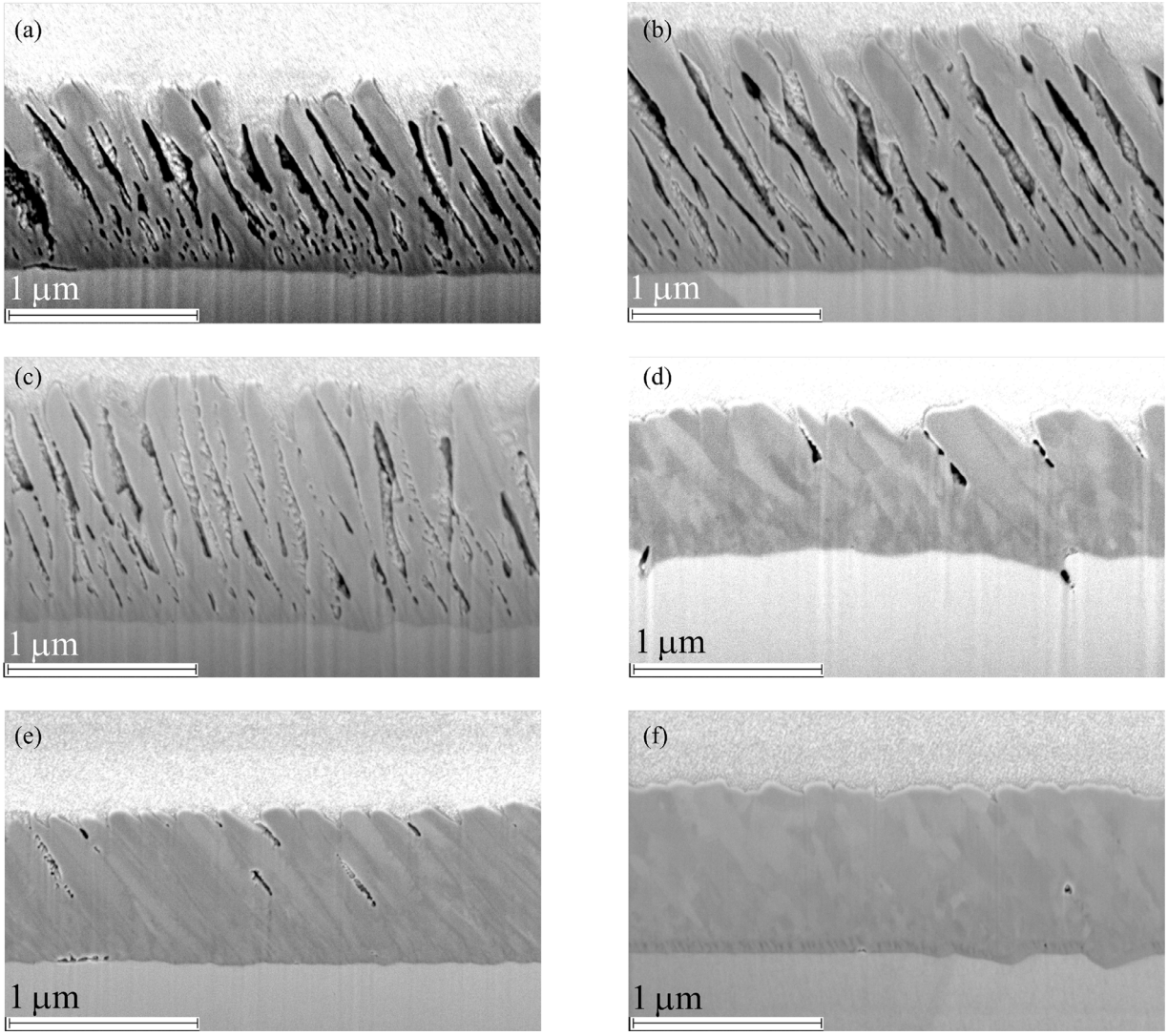


**Fig. 5.** Nb films FIB cross sections of samples at 90° coated in: (a) DCMS with grounded substrate, (b) DCMS with −50 V biased substrate, (c) HiPIMS with grounded substrate, (d) HiPIMS with −50 V biased substrate, (e) HiPIMS with grounded substrate and +50 V PP, (f) HiPIMS with grounded substrate and +100 V PP.

**Table 2**
Critical temperature $T_c$ and width of the transition Δ for the Nb/Cu coated films at 0° and 90° incidence angles. *S* refers to the SQUID method. *I* refers to the inductive method implemented at the CERN $T_c$ test-stand. N.a. stands for not available data.

| | | | 0° | | | | 90° | | | |
|---|---|---|---|---|---|---|---|---|---|---|
| | | | $T_c$ [K] | | Δ [K] | | $T_c$ [K] | | Δ [K] | |
| Process | Sub. Bias [V] | PP [V] | *S* | *I* | *S* | *I* | *S* | *I* | *S* | *I* |
| DCMS | 0 | – | 6.34 | 6.5 | 0.28 | 0.97 | no transition | | | |
| DCMS | −50 | – | 8.89 | n.a. | 0.05 | n.a. | 7.07 | n.a. | 0.36 | n.a. |
| HiPIMS | 0 | 0 | 8.85 | 9.0 | 0.09 | 0.08 | 7.29 | 6.8 | 0.18 | 1.36 |
| HiPIMS | −50 | 0 | 8.87 | 9.1 | 0.16 | 0.30 | 8.94 | 8.6 | 0.07 | 0.70 |
| HiPIMS | 0 | +50 | 9.05 | 9.16 | 0.12 | 0.34 | 8.29 | 7.0 | 0.09 | 0.74 |
| HiPIMS | 0 | +100 | 9.0 | 9.1 | 0.06 | 0.10 | 9.0 | 8.7 | 0.04 | 0.38 |

impinging particles plays a crucial role for the performances of the SRF cavities with Nb/Cu coatings [5], together with other aspects, including the micro-structure and the presence of impurities. Elliptical SRF cavities designed for different sections of the accelerators, corresponding to different particle types and speeds, feature geometries such that the coating of the inner surface presents variable angles of incidence of the Nb particles down to grazing angles. The performance of such cavities could be strongly related to the incidence angle of the sputtered Nb atoms on the Cu surface, as mentioned in previous studies [36,37]. Cavities with more complex geometries featuring concave and convex shapes present the same inconvenience [38]. To validate the PP approach for the coating of SRF cavities with dense and void-free Nb thin films, the first step is the measurement of the superconducting critical temperature $T_c$. The herein $T_c$ values are measured using both a Quantum Design Magnetic Property Measurement System (MPMS) SQUID Vibrating Sample Magnetometers (VSMs) at the University of Geneva [39], and the $T_c$ test-stand at the CERN Central Cryogenic Laboratory, which is based on an inductive technique. More details on the experimental setups and data analysis are provided in Appendix A. A summary of the results is given in Table 2.

Of particular interest are the samples coated at 90°, where no transitions or a $T_c$ close to 7 K are measured for films coated in DCMS and HiPIMS without substrate bias nor PP, while higher values close to 9 K are obtained for HiPIMS with either the biased substrate or the PP. The closest $T_c$ to the 9.2 K expected for bulk Nb is given by the implementation of HiPIMS with a −50 V bias and with a PP of +100 V. This result is consistent with the improved density of the film observed in the FIB cross sections. Further analysis will address the lower $T_c$ measured for the HiPIMS with a PP of +50 V. The width of the

transitions obtained from SQUID analysis for the samples at 0° are all below 0.2 K, with the exception of the DCMS coating without biased substrate where a wider transition is associated to the presence of two critical temperatures. This might be caused by the two consecutive coatings performed on the same sample to reach the target thickness, with an intermediate venting and consequent formation of an oxide layer. The biggest discrepancy with respect to the inductive technique is also observed for this sample. Samples at 90° show transition widths that are similar to those at 0° for the SQUID technique, while wider transitions are measured with the inductive technique. This might be related to the local feature of SQUID measurements, while the inductive technique provides information averaged on the whole sample surface. We note that Nb/Cu coatings of SRF cavities require a preliminary cavity and ultra high vacuum system baking to meet the SRF requirements of cleanliness. For the herein discussed coatings, baking was not performed as the SRF characterization is not possible on samples with this geometry. Cleanliness might affect the measured $T_c$, but all the coatings have been performed in the same conditions, allowing the relative comparison that we have discussed. We also remark that the presence of high-energy gas ions might lead to an increased incorporation of gas atoms in the deposited film. This could affect the SRF properties of the films, and therefore dedicated studies should address this topic.

## 6. Conclusions

In this work, niobium on copper coatings were performed on samples parallel (0°) and perpendicular (90°) to the sputtering target surface. This allowed to investigate the effect of the incident angle of the impinging atoms on the film morphology and structural properties with the comparison of different sputtering techniques. Similar features can be observed for samples at 0°, with dense and void-free films. Significant differences are evident for samples coated at 90°. Porous films are observed in DCMS, and HiPIMS with grounded substrate and without a PP. For films coated in HiPIMS with the application of a negative bias to the substrate (−50 V) or a PP after the main negative pulse (+50 V), a denser film is obtained. This can be explained with the acceleration of $Nb^+$ and $Ar^+$ species towards the substrate that promote the adatom surface mobility during the film growth. This feature is more effective with a PP voltage of +100 V. These results are relevant for the whole thin-film community to improve the densification in the coating of objects with large and complex shapes featuring surfaces at grazing angles of incidence. In the framework of the application of HiPIMS with a PP for the Nb/Cu coating of SRF cavities, measurements of the superconducting critical temperature of the coated films are provided. For the most challenging configuration of 90° incidence angle, $T_c$ values close to the reference bulk Nb of 9.2 K are obtained in HiPIMS with a substrate bias and with a PP. This validates at this sample scale the alternative process of HiPIMS with PP for SRF applications. Further studies shall be performed focusing on film stress, on the quantification of gas inclusion as a consequence of the acceleration of gas ions, as well as on the correlation between gas inclusion and SRF performances.

## CRediT authorship contribution statement

**F. Avino:** . **D. Fonnesu:** Data curation, Formal analysis, Writing - original draft, Investigation. **T. Koettig:** Supervision, Resources. **M. Bonura:** Data curation, Formal analysis, Investigation. **C. Senatore:** Supervision, Project administration, Resources. **A.T. Perez Fontenla:** Data curation, Formal analysis, Writing - original draft, Investigation. **A. Sublet:** Conceptualization, Investigation, Supervision, Project administration, Writing - original draft, Writing - review & editing. **M. Taborelli:** Conceptualization, Investigation, Supervision, Project administration, Writing - original draft, Writing - review & editing.

## Declaration of Competing Interest

The authors declare that they do not have any financial or non-financial conflict of interests.

## Acknowledgements

The authors wish to acknowledge the receipt of the Marie Sklodowska-Curie fellowships as part of the EU-funded project COFUND-FP-CERN-2014 and the EASITrain Programme.[1] Authors are also thankful to the TE-VSC group at CERN for the very helpful discussions, in particular to G. Rosaz, T. Richard, S. Calatroni, P. Costa Pinto and A. Lunt for FIB-SEM measurements. Many thanks to the EPFL-SPC for the loan of the MEA.

## Appendix A. $T_c$ measurement techniques and data analysis

### A1. SQUID

A Superconducting QUantum Interference Device (SQUID) is based on superconducting loops containing Josephson junctions, and it allows to measure extremely low magnetic fields. For the herein results, speed and sensitivity of the measurements performed with the SQUID Vibrating Sample Magnetometer (VSM) are optimized by vibrating the sample at a known frequency and by employing phase-sensitive detection for rapid data collection and spurious signal rejection. Unlike traditional VSMs, the size of the signal produced by a sample is not dependent on the frequency of vibration, but only on the magnetic moment of the sample, the vibration amplitude, and the design of the SQUID detection circuit. The SQUID VSM is equipped with a superconducting coil able to generate magnetic fields up to 7 T and the sample temperature can be regulated between 1.8 and 400 K. To get rid of the residual flux possibly trapped in the superconducting coil, the latter was quenched before starting the zero-field cooling procedure. Each sample was zero-field cooled before measurement. Measurements of magnetic moment (m) as a function of the sample temperature (T) are performed in the range 2.5–11 K at $B = 1.2 \times 10^{-3}$ T, with a temperature sweep rate 1 K/min. The curve corresponding to the samples coated in HiPIMS with +100 V PP is shown in Fig. A.1. A Gaussian fit is performed on the derivative of the magnetic momentum curve, which is calculated between two consecutive measured points. An example of analysis is shown in the inset of Fig. A.1. The $T_c$ and the width $\Delta$ of the transition are evaluated as the maximum and the FWHM of the resulting fit, respectively.

### A2. Inductive technique at CERN

The $T_c$ test-stand at CERN is based on a contact-less technique where the sample is placed between two coils arranged in front of each other, the

[1] EASITrain – European Advanced Superconductivity Innovation and Training. This Marie Sklodowska-Curie Action (MSCA) Innovative Training Networks (ITN) has received funding from the European Union's H2020 Framework Programme under Grant Agreement no. 764879

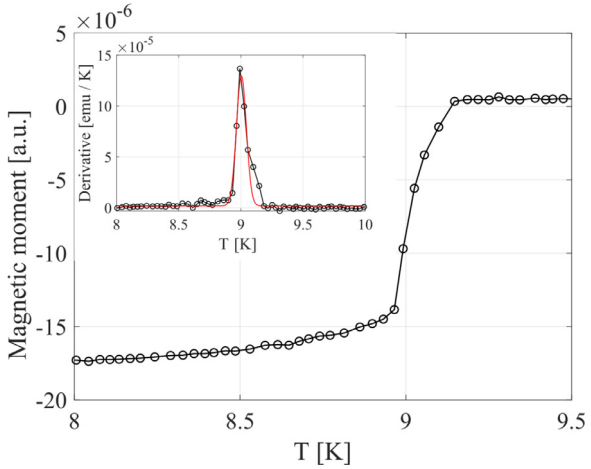


**Fig. A1.** SQUID measurement of the normal conducting to superconducting transition of the grounded sample coated at 90° in HiPIMS with +100 V PP. In the inset, the corresponding calculated derivative with the Gaussian fit (in red).

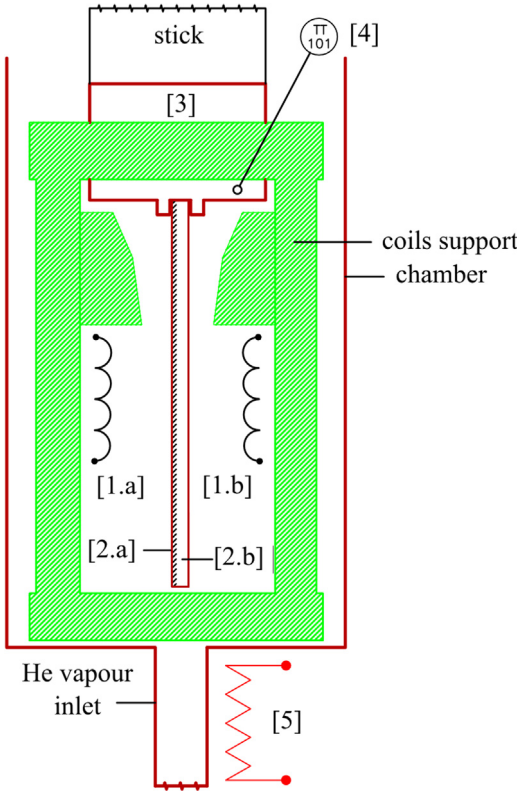


**Fig. A2.** Scheme of the $T_c$ test-stand experimental setup. In evidence: the two coils [1.a] and [1.b], the copper substrate of the sample [2.b] with the niobium film [2.a], the holder [3], the temperature sensor [4], and the heater [5]. The setup lies above a liquid He bath, in He vapor environment. The sample can be placed between the coils from the top of the chamber, through a stick that can slide down the cryostat insert.

coil planes having opposite orientations and being parallel to the surface of the sample, as illustrated in Fig. A.2. The coil facing the thin-film, namely the *drive* coil ([1,a]), is excited with a sinusoidal AC current that in turn generates an alternating magnetic field. This field can be detected, as induced voltage, by the passive *pickup* coil ([1,b]) facing the sample substrate. When the film ([2,a]) is superconducting, the external magnetic field is expelled by the intense screening currents induced on its surface. On the contrary, when the sample is in the normal conducting state, the eddy currents induced on the sample are not strong enough to shield the field such that the sample is transparent to the magnetic field (given that the frequency of the drive current is low enough for the skin depth of the Cu substrate to stay much larger than its thickness). A voltage proportional to the change rate of the magnetic flux through the pickup coil and to the coils mutual inductance is consequently induced in the pickup coil. The coils are arranged on a glass fiber epoxy support ([3]) placed inside a copper chamber. The chamber, mounted at the bottom-end of a liquid He bath cryostat insert, lies above the helium level in helium vapor environment. The thin-film sample, mounted on a copper holder, is lowered inside the chamber with a stick that can slide inside the cryostat insert. In order to cool down the sample, the vapor can flow inside the chamber through an inlet at its bottom, its temperature being adjusted by a copper wire heater ([5]) wound around the vapor inlet. The temperature of the sample is monitored by a Cernox sensor ([4]) placed inside the sample holder.

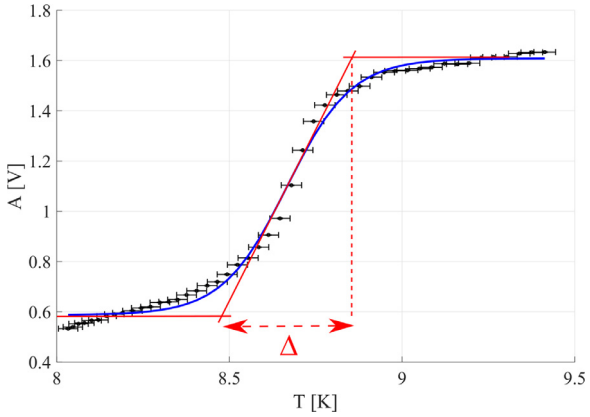


**Fig. A3.** Coil measurement of the superconducting to normal conducting transition of grounded sample coated at 90° in HiPIMS with +100 V PP. The data points of the voltage amplitude of the *pickup* coil are shown in black with their error bars as a function of the average temperature. The data fit is displayed with a continuous blue curve. In red, the lines for the estimate of the transition width Δ.

To measure the $T_c$ of the film, the sample is first cooled down to 4.5–5 K, which is the lowest temperature range reachable with this setup. This is performed in the absence of external magnetic fields to avoid any possible flux trapping which might affect the temperature and the properties of the signal shape of the transition. Once the temperature is stable within 0.1 K, the drive signal is turned on and the acquisition of the voltage signal in the pickup coil is started. The standard duration of one measurement is 30 minutes and the initial settings for the heater and helium flow across the sample chamber are chosen in such a way that the temperature of the sample increases homogeneously during the measurement and rises above $T_c$ at approximately half of the measurement time interval. This allows to obtain symmetric data around the superconducting to normal conducting transition. The temperature of the sample and the voltage in the pickup coil are recorded simultaneously. $T_c$ is extracted by sampling in time the data sets into sub-intervals equal in size, typically 1 s. An average temperature $\langle T \rangle$ is obtained from each temperature sub-interval, and a corresponding voltage amplitude $A(\langle T \rangle)$ is evaluated by fitting each pickup voltage signal sub-interval. The voltage amplitude $A(\langle T \rangle)$ is then plotted against the average temperature $\langle T \rangle$ and fitted with a four-parameters logistic curve given by:

$$A(\langle T \rangle) = \frac{L}{1 + e^{-a(\langle T \rangle - T_c)}} + C \tag{A.1}$$

which reflects the step-like trend of the transition signal, and allows the extraction of $T_c$ as the fit parameter representing the temperature corresponding to the half-height of the transition step.

The width of the transition is calculated as the temperature difference between the two points obtained from the intersection of the tangent to the fit curve at the inflection point (corresponding to $T_c$), and the lines corresponding to the voltage amplitude before and after the transition. The data and the fit curve implemented for the extraction of $T_c$ (blue) and the procedure to obtain Δ (red) are shown in Fig. A.3 for the film coated in HiPIMS with $+100\,V$ PP and 90° incident angle.

## References


[1] G. Greczynski, J. Jensen, L. Hultman, CrNx films prepared by DC magnetron sputtering and high-power pulsed magnetron sputtering: a comparative study, IEEE Trans. Plasma Sci. 38 (2010), https://doi.org/10.1109/TPS.2010.2071885.

[2] J. Lin, R. Wei, A comparative study of thick TiSiCN nanocomposite coatings deposited by dcMS and HiPIMS with and without PEMS assistance, Surf. Coat. Technol. 338 (2018) 84, https://doi.org/10.1016/j.surfcoat.2018.01.082.

[3] L. Abelmann, C. Lodder, Oblique evaporation and surface diffusion, Thin Solid Films 305 (1997) 1, https://doi.org/10.1016/s0040-6090(97)00095-3.

[4] M. Wu, J. Moulin, A. Bosseboeuf, Oblique angle deposition of Au/Ti porous getter films, J. Appl. Phys. 124 (2018) 55301, https://doi.org/10.1063/1.5044570.

[5] S. Calatroni, 20 years of experience with the Nb/Cu technology for superconducting cavities and perspectives for future developments, Phys. C 441 (2006) 95, https://doi.org/10.1016/j.physc.2006.03.044.

[6] J. Alami, P.O. Persson, D. Music, J.T. Gudmundsson, J. Bohlmark, U. Helmersson, Ion-assisted physical vapor deposition for enhanced film properties on nonflat surfaces, J. Vac. Sci. Technol. A 23 (2005) 278, https://doi.org/10.1116/1.1861049.

[7] T. Nakano, N. Hirukawa, S. Saeki, S. Baba, Effects of target voltage during pulse-off period in pulsed magnetron sputtering on afterglow plasma and deposited film structure, Vacuum 87 (2013) 109, https://doi.org/10.1016/j.vacuum.2012.03.010.

[8] A.P. Ehiasarian, W.-D. Munz, L. Hultman, U. Helmersson, I. Petrov, High power pulsed magnetron sputtered CrNx films, Surf. Coat. Technol. 163–164 (2003) 267, https://doi.org/10.1016/S0257-8972(02)00479-6.

[9] A.P. Ehiasarian, W.P.E. Hovsepian, L. Hultman, U. Helmersson, Comparison of microstructure and mechanical properties of chromium nitride-based coatings deposited by high power impulse magnetron sputtering and by the combined steered cathodic arc/unbalanced magnetron technique, Thin Solid Films 457 (2004) 270, https://doi.org/10.1016/j.tsf.2003.11.113.

[10] I.-L. Velicu, V. Tiron, C. Porosnicu, I. Burducea, N. Lupu, G. Stoian, G. Popa, D. Munteanu, Enhanced properties of tungsten thin films deposited with a novel HiPIMS approach, Appl. Surf. Sci. 424 (2017) 397, https://doi.org/10.1016/j.apsusc.2017.01.067.

[11] P.E. Hovsepian, A.P. Ehiasarian, Y.P. Purandare, B. Biswas, F.J. Pérez, M.I. Lasanta, M.T. de Miguel, A. Illana, M. Juez-Lorenzo, R. Muelas, A. Aguero, Performance of HIPIMS deposited CrN/NbN nanostructured coatings exposed to 650 °C in pure steam environment, Mater. Chem. Phys. 179 (2016) 110, https://doi.org/10.1016/j.matchemphys.2016.05.017.

[12] S. Rtimi, O. Baghriche, C. Pulgarin, A. Ehiasarian, R. Bandorf, J. Kiwi, Comparison of HIPIMS sputtered Ag- and Cu-surfaces leading to accelerated bacterial inactivation in the dark, Surf. Coat. Technol. 250 (2014) 14, https://doi.org/10.1016/j.surfcoat.2014.02.029.

[13] M. Drábik, V. Ballo, M. Truchlý, J. Frkán, T. Roch, L. Kvetková, L. Satrapinskyy, P. Kús, Influence of plasma pretreatment on the performance of industrial tungsten carbide coatings deposited at low temperature on 100Cr6 bearing steel substrates, Surf. Coat. Technol. 293 (2016) 2, https://doi.org/10.1016/j.surfcoat.2016.01.035.

[14] V. Tiron, I.-L. Velicu, I. Pana, D. Cristea, B.G. Rusu, P. Dinca, C. Porosnicu, E. Grigore, D. Munteanu, S. Tascu, HiPIMS deposition of silicon nitride for solar cell application, Surf. Coat. Technol. 344 (2018) 197, https://doi.org/10.1016/j.surfcoat.2018.03.025.

[15] S. Konstantinidis, J.P. Dauchot, M. Hecq, Titanium oxide thin films deposited by high-power impulse magnetron sputtering, Thin Solid Films 515 (2006) 1182, https://doi.org/10.1016/j.tsf.2006.07.089.

[16] G. Terenziani, S. Calatroni, T. Junginger, I.A. Santillana, A.P. Ehiasarian, Nb coating developments with HIPIMS for SRF applications, Proceedings of SRF, (2013), p. 627.

[17] L. Phillips, K. Macham, A.M. Valente-Feliciano, Design and commissioning status of new cylindrical HiPIMS Nb coating system for SRF cavities, Proceedings of SRF, (2013), p. 617.

[18] M. Audronis, A. Leyland, P.J. Kelly, A. Matthews, The effect of pulsed magnetron sputtering on the structure and mechanical properties of CrB2 coatings, Surf. Coat. Technol. 201 (2006) 3970, https://doi.org/10.1016/j.surfcoat.2006.08.006.

[19] J.-W. Lee, S.-K. Tien, Y.C. Kuo, The effects of pulse frequency and substrate bias to the mechanical properties of CrN coatings deposited by pulsed DC magnetron

sputtering, Thin Solid Films 494 (2006) 161, https://doi.org/10.1016/j.tsf.2005.07.190.
[20] G. Lanza, J. Bermudez, A. Frigo, H. Padamsee, V. Palmieri, D. Tonini, New magnetron configurations for sputtered Nb onto Cu, Phys. C 441 (2006) 102, https://doi.org/10.1016/j.physc.2006.03.041.
[21] G. Greczynski, J. Lu, S. Bolz, W. Kölker, C. Schiffers, O. Lemmer, I. Petrov, J.E. Green, L. Hultman, Novel strategy for low-temperature, high-rate growth of dense, hard, and stress-free refractory ceramic thin films, J. Vac. Sci. Technol. A 32 (2014) 41515, https://doi.org/10.1116/1.4884575.
[22] N. Britun, M. Michiels, T. Godfroid, R. Snyders, Ion density evolution in a high-power sputtering discharge with bipolar pulsing, Appl. Phys. Lett. 112 (2018) 234103, https://doi.org/10.1063/1.5030697.
[23] B. Wu, I. Haehnlein, I. Shchelkanov, J. McLain, D. Patel, J. Uhlig, B. Jurczyk, Y. Leng, D.N. Ruzic, Cu films prepared by bipolar pulsed high power impulse magnetron sputtering, Vacuum 150 (2018) 216, https://doi.org/10.1016/j.vacuum.2018.01.011.
[24] A. Anders, Tutorial: Reactive high power impulse magnetron sputtering (R-HiPIMS), J. Appl. Phys. 121 (2017) 171101, https://doi.org/10.1063/1.4978350.
[25] G. Eichenhofer, I. Fernandez-Martinez, A. Wennberg, Industrial use of HiPIMS up to now and a glance into the future, a review by a manufacturer introduction of the hiP-V hiPlus technology, Univ. J. Phys. Appl. 11 (2017) 73–79, https://doi.org/10.13189/ujpa.2017.110301.
[26] G. Eichenhofer, I. Fernandez-Martinez, M. Banghard, C.D.L. Viesca, The implementation of a reversed voltage pulse technology enables enhanced coating properties for glass, plastics, fiber and other non-conductive substrates. A special consideration of this work will be given to medical coatings of biocompatible polymers on implantable devices, 9th Int. Conf. on HiPIMS, (2018).
[27] S. Konstantinidis, J.P. Dauchot, M. Ganciu, M. Hecq, Transport of ionized metal atoms in high-power pulsed magnetron discharges assisted by inductively coupled plasma, Appl. Phys. Lett. 88 (2006) 021501, https://doi.org/10.1063/1.2162671.
[28] J. Alami, K. Sarakinos, G. Mark, M. Wuttig, On the deposition rate in a high power pulsed magnetron sputtering discharge, Appl. Phys. Lett. 89 (2006) 154104, https://doi.org/10.1063/1.2362575.
[29] A. Anders, Self-sputtering runaway in high power impulse magnetron sputtering: the role of secondary electrons and multiply charged metal ions, Appl. Phys. Lett. 92 (2008) 201501, https://doi.org/10.1063/1.2936307.
[30] P. Klein, J. Hnilica, Z. Hubicka, M. Cada, M. Slapanska, M. Zemanek, P. Vasina, Cathode voltage and discharge current oscillations in HiPIMS, Plasma Sources Sci. Technol. 26 (2017) 55015, https://doi.org/10.1088/1361-6595/aa62ee.
[31] S.M. Meier, A. Hecimovic, T.V. Tsankov, D. Luggenholscher, U. Czarnetzki, First measurements of the temporal evolution of the plasma density in HiPIMS discharges using THz time domain spectroscopy, Plasma Sources Sci. Technol. 27 (2018) 35006, https://doi.org/10.1088/1361-6595/aab188.
[32] F. Avino, A. Sublet, M. Taborelli, Evidence of ion energy distribution shift in HiPIMS plasmas with positive pulse, Plasma Sources Sci. Technol. 28 (2019) 01LT03, https://doi.org/10.1088/1361-6595/aaf5c9.
[33] J. Keraudy, R.P.B. Viloan, M. Raadu, N. Brenning, D. Lundin, U. Helmersson, Bipolar HiPIMS for tailoring ion energies in thin film deposition, Surf. Coat. Technol. 359 (2019) 433, https://doi.org/10.1016/j.surfcoat.2018.12.090.
[34] R.P.B. Viloan, J. Gu, R. Boyd, J. Keraudy, L. Li, U. Helmersson, Bipolar high power impulse magnetron sputtering for energetic ion bombardment during TiN thin film growth without the use of a substrate bias, Thin Solid Films 688 (2019) 137350, https://doi.org/10.1016/j.tsf.2019.05.069.
[35] G. Greczynski, I. Petrov, J.E. Greene, L. Hultman, Paradigm shift in thin-film growth by magnetron sputtering: from gas-ion to metal-ion irradiation of the growing film, J. Vac. Sci. Technol. A 37 (2019) 60801, https://doi.org/10.1116/1.5121226.
[36] C. Benvenuti, D. Boussard, S. Calatroni, E. Chaiveri, J. Tückmantel, Production and test of 352 MHz niobium sputtered reduced beta cavities, in: Proceedings of the 1997 Workshop on RF Superconductivity, p. 1038.
[37] O. Aberle, D. Boussard, S. Calatroni, E. Chiaveri, E. Haebel, R. Hanni, R. Losito, S. Marque, J. Tückmantel, Technical developments on reduced-β superconducting cavities at CERN, in: Proceedings of the 1999 Particle Accelerator Conference, p. 949.
[38] A. Grudiev, S. Atieh, R. Calaga, S. Calatroni, O. Capatina, F. Carra, G. Favre, L.M.A. Ferreira, J.-F. Poncet, T. Richard, A. Sublet, C. Zanoni, Design of a compact superconducting crab-cavity for LHC using Nb-on-Cu-coating technique, in: Proceedings of the 2015 Workshop on RF Superconductivity, (2015) 1205.
[39] Magnetic property measurement system. quantum design MPMS 3 user's manual, 2010. Part Number 1500-100, E0.